Operational Implementation of the ISBA Land Surface Scheme in the Canadian Regional Weather Forecast Model. Part I: Warm Season Results

STÉPHANE BÉLAIR

Meteorological Research Branch, Meteorological Service of Canada, Dorval, Quebec, Canada

LOUIS-PHILIPPE CREVIER

Canadian Meteorological Centre, Meteorological Service of Canada, Dorval, Quebec, Canada

JOCELYN MAILHOT, BERNARD BILODEAU, AND YVES DELAGE

Meteorological Research Branch, Meteorological Service of Canada, Dorval, Quebec, Canada

(Manuscript received 12 April 2002, in final form 15 October 2002)

ABSTRACT

The summertime improvement resulting from the operational implementation of a new surface modeling and assimilation strategy into the Canadian regional weather forecasting system is described in this study. The surface processes over land are represented in this system using the Interactions between Soil–Biosphere–Atmosphere (ISBA) land surface scheme. Surface variables, including soil moisture, are initialized using a sequential assimilation technique in which model errors of low-level air temperature and relative humidity are used to determine analysis increments of surface variables.

It was found that the magnitude and nature of the analysis increments applied to the surface variables depended on the surface and meteorological conditions observed in each region. In regions characterized by weak meteorological activity (i.e., no clouds or precipitation), model errors of low-level air characteristics are more likely to be related to an incorrect representation of surface processes due to either erroneous initial conditions or inaccurate parameterizations in the land surface scheme. In other regions characterized by more frequent and more intense precipitation events, surface corrections are mainly associated with inaccurate atmospheric forcing.

Objective evaluation against observations from radiosondes and surface stations showed that the amplitude of the diurnal cycle of near-surface air temperature and humidity is larger with the new surface system, in better agreement with observations. This type of improvement was found to extend higher up in the boundary layer (up to 700 hPa) where cold and humid biases were significantly reduced by introducing the new surface system. The model precipitation was also found to be significantly influenced by the new representation of surface fluxes. The problematic increase of a positive bias in precipitation with integration time was found to be significantly reduced with the new system, due to the warmer and drier boundary layer.

1. Introduction

The importance of accurately representing exchanges of heat, moisture, and momentum between the surface and the overlying atmosphere has long been recognized in general circulation modeling (Charney et al. 1977; Shukla and Mintz 1982; Sud et al. 1988). It has often been shown, for instance, that surface fluxes significantly influence medium- and long-range prediction of low-level temperature and humidity (e.g., Rowntree and Bolton 1983; Yang et al. 1994; Huang et al. 1996; Fennessy and Shukla 1999), and precipitation (Beljaars et al. 1996; Paegle et al. 1996; Eltahir 1998; Schär et al. 1999).

In the context of shorter-range numerical weather prediction, the role of surface exchanges are important for the diurnal evolution of the boundary layer (see Pan and Mahrt 1987; Ek and Mahrt 1994), for conditioning prestorm environments (see Lanicci et al. 1987; Chang and Wetzel 1991), and for the triggering and intensity of convective activity (e.g., Clark and Arritt 1995; Gallus and Segal 2000). Other studies have demonstrated the impact of soil moisture (which plays a major role in the partitioning of net incoming radiation at the surface into sensible, latent, and ground heat fluxes) on mesoscale atmospheric circulations, such as drylines (Ziegler et al. 1995; Grasso 2000), squall lines (Koch et al. 1997), and low-level jets (McCorcle 1988; Fast and McCorcle 1991).

Corresponding author address: Dr. Stéphane Bélair, Recherche en Prévision Numérique, 2121 Trans-Canada Highway, Room 500, Dorval, QC H9P 1J3, Canada.
E-mail: stephane.belair@ec.gc.ca

Considerable efforts have been made in the last decade to improve the representation of surface fluxes and the initialization of soil moisture in atmospheric models. A multitude of surface–vegetation–atmosphere transfer (SVAT) schemes of varying levels of complexity has been developed like, for example, the Biosphere–Atmosphere Transfer scheme (BATS; Dickinson et al. 1986), the Simple Biosphere model (SiB; Sellers et al. 1986), the Interactions between Soil–Biosphere–Atmosphere (ISBA) scheme (Noilhan and Planton 1989), the Canadian Land Surface Scheme (CLASS; Verseghy 1991), and many others. A description and comparison of SVAT schemes is provided by Chen et al. (1997).

Several techniques for initializing soil moisture have been proposed and used, ranging from optimal interpolation (see Mahfouf 1991) or variational assimilation (see Mahfouf 1991; Callies et al. 1998; Hess 2001) using low-level atmospheric observations, to direct assimilation of microwave radiances (see Entekhabi et al. 1994).

In the 1990s, several national weather forecasting centers took advantage of these advancements by operationally implementing new surface modeling and assimilation systems. The European Centre for Medium-Range Weather Forecasts (ECMWF) implemented a four-level surface scheme with a simple representation of vegetation (Viterbo and Beljaars 1995). A simple ''nudging'' technique was included in their operational suite to prevent long-term drift of soil moisture. At Météo-France, the ISBA surface scheme was implemented in the short- and medium-range weather forecasting models, together with a sequential assimilation strategy based on the work of Mahfouf (1991) and Bouttier et al. (1993a,b) (see Giard and Bazile 2000). In the United States, the National Centers for Environmental Prediction (NCEP) opted for implementing a modified version of the Oregon State University (OSU) surface scheme (see Pan and Mahrt 1987; Chen et al. 1996). For initializing soil moisture, NCEP is currently developing what is called the ''Land Data Assimilation System'' (LDAS), in which several surface schemes are integrated in an ''offline'' manner, using the best possible estimates for atmospheric forcing (i.e., low-level temperature, humidity, and wind, as well as incoming radiation and precipitation) (see Mitchell et al. 2000).

In this study, we present the initial verification results that led to the operational implementation in September 2001 of a new surface modeling system at the Canadian Meteorological Centre (CMC). This new system includes the ISBA surface scheme and a sequential assimilation cycle based on Mahfouf (1991), Bouttier et al. (1993a), and Giard and Bazile (2000). The main objectives of this study are to (i) quantify the impact of better representing surface processes on summertime short-range weather forecasting, (ii) examine the role and importance of the soil moisture initialization technique, and (iii) discuss the potential use of diagnostics from the sequential assimilation cycle (i.e., model errors and increments) to acquire information concerning the systematic errors of the atmospheric model.

TABLE 1. Summary of the operational GEM regional forecast system.

Dynamics/numerics
• hydrostatic primitive equations
• global variable–resolution grid (horizontal and vertical)
• cell-integrated finite-element discretization on Arakawa-C grid
• terrain-following hydrostatic pressure vertical coordinate
• two-time-level semi-implicit time scheme
• 3D semi-Lagrangian advection
• linear ∇^2 horizontal diffusion on all model variables, except specific humidity
• periodic horizontal boundary conditions
• no motion across the lower and upper boundaries
Physics
• planetary boundary layer based on TKE
• fully implicit vertical diffusion
• stratified surface layer, distinct roughness lengths for momentum and heat/humidity
• four types of surface represented: continent, water, sea ice, and glaciers
• ISBA surface scheme for land surface processes
• solar/infrared radiation schemes with cloud–radiation interactions based on predicted cloud radiative properties
• Fritsch–Chappell convective scheme
• Sundqvist scheme for grid-scale condensation
Regional data assimilation system
• 12-h data assimilation cycle with 6-h trial field from regional GEM
• incremental 3DVAR algorithm
• innovations computed with respect to background field at the full model resolution
• analysis increments produced on a 240 × 120 (T108 spectral resolution) global Gaussian grid
• analysis on model levels
• initialization by a diabatic digital filter

In the paper, we first describe the Global Environmental Multiscale (GEM) atmospheric model, which is currently used operationally at CMC for short-range weather forecasting (section 2). The ISBA surface scheme is then described (section 3), as well as the sequential assimilation technique (section 4). Results concerning the role of the assimilation technique and the impact of the new surface modeling system are presented in section 5. A summary and conclusions are given in the final section of the paper.

2. The GEM atmospheric model

Since February 1997, the Canadian short-range regional forecasting system is based on the GEM model (Côté et al. 1993; 1998a,b; see Table 1), in which the primitive hydrostatic equations are integrated on a global variable-resolution grid (Arakawa-C type) using the semi-implicit and semi-Lagrangian numerical techniques. This regional version of GEM has a uniform horizontal resolution of 0.22° (~24 km) in the central portion of the model grid, which covers North America and the adjacent waters (see Fig. 1 of Bélair et al. 2000). The vertical resolution is also varying, with a greater

concentration of levels in the boundary layer. A terrain-following normalized pressure coordinate is used (Phillips 1957; Kasahara 1974), and no motion is allowed across the surface and top levels.

The initial atmospheric conditions are provided by a regional data assimilation system (RDAS), with 12-h cycles using trial fields from 6-h regional GEM integrations (see, Chouinard et al. 1994). Data assimilation in RDAS is done using a three-dimensional variational technique (Laroche et al. 1999). The analysis is based on the incremental method (Courtier et al. 1994), in which the full resolution of the regional model is taken into account for the innovations (i.e., differences between observations and the background fields), while analysis increments are produced on a lower-resolution global Gaussian grid.

In the previous operational version of GEM, the representation of surface processes was based on a simplified force–restore strategy in which vegetation and snow were treated in a crude manner and in which only the surface temperature T_S evolves prognostically (see Mailhot et al. 1997; 1998), following

$$\frac{\partial T}{\partial t} = C_{\mathrm{TFR}}(R_n - H - \mathrm{LE}) - \frac{2\pi}{\tau}(T_S - T_p) \quad (1)$$

in which C_{TFR} is a constant that describes the thermal characteristics of the soil; R_n, H, and LE are the net radiation, sensible heat, and latent heat fluxes at the surface, respectively; τ is a 1-day time constant; and T_p is a deep soil temperature, kept constant during the integrations. Soil moisture availability was also kept constant during model integrations and was initialized using an error feedback mechanism, not unlike the strategy described later in section 4, which utilizes the model errors on low-level dewpoint depression to diagnose analysis increments for the soil moisture variable (i.e., the soil moisture availability factor; see Mailhot et al. 1997).

GEM's physics package also includes (a) solar and infrared radiation, fully interactive with clouds (Fouquart and Bonnel 1980; Garand 1983), (b) implicit vertical diffusion with K coefficients obtained from a turbulent mixing length and from a prognostic turbulent kinetic energy (TKE) (Benoit et al. 1989), (c) a mass-flux deep convective scheme based on the removal of convective available potential energy (CAPE) (Fritsch and Chappell 1980; Bélair et al. 2000), and (d) a grid-scale condensation scheme based on Sundqvist (1978) (see also Pudykiewicz et al. 1992).

3. The ISBA land surface scheme

In the new surface modeling system included in GEM, surface fluxes are calculated over four types of surface: land, water, glaciers, and sea ice. The effective fluxes used as a lower boundary condition for the boundary layer vertical diffusion are derived from an area-weighted aggregation of the fluxes over the four surface types. The main emphasis of this study is to examine the summertime performance of the ISBA surface scheme over land. The other schemes for processes over sea ice and glaciers will be the subject of forthcoming publications. (Over water bodies, the surface temperature is provided by an analysis and is kept constant during the model integrations.)

TABLE 2. ISBA's prognostic variables.

Variable	Definition	Units
T_S	Surface temperature	K
T_2	Mean surface temperature	K
w_g	Superficial (first 10 cm) volumetric water content	$m^3\ m^{-3}$
w_2	Rooting depth volumetric water content	$m^3\ m^{-3}$
W_r	Liquid water retained on the vegetation canopy	Kg m^{-2}
W_S	Snow mass	Kg m^{-2}
α_S	Snow albedo	
ρ_S	Snow density (relative to water density)	
W_L	Liquid water in the snowpack	Kg m^{-2}
w_F	Volumetric content of frozen soil water	$m^3\ m^{-3}$

The ISBA surface scheme was developed in the late 1980s at Météo-France (see Noilhan and Planton 1989) and was tested over a wide variety of surface types (e.g., Jacquemin and Noilhan 1990; Braud et al. 1993; Calvet et al. 1999; Habets et al. 1999). Many versions of ISBA, of varying degrees of complexity (see Boone et al. 1999, 2000), are used nowadays. A description of the version implemented at CMC is provided below.

The 10 variables that evolve prognostically in CMC's version of ISBA are listed in Table 2. Because the focus of the present study is on ISBA's summertime performance, the prognostic equations for T_S, T_2, w_g, w_2, and W_r are described in the rest of this section. Details concerning ISBA's treatment of cold climate (winter) processes are given in Bélair et al. (2003).

The prognostic equations for the surface temperature T_S and the mean surface temperature T_2 are obtained from the force–restore method (Bhumralkar 1975):

$$\frac{\partial T_S}{\partial t} = C_T(R_n - H - \mathrm{LE}) + C_T L_f(\mathrm{freez}_g - \mathrm{melt}_g + \mathrm{freez}_S - \mathrm{melt}_S) - \frac{2\pi}{\tau}(T_S - T_2), \quad (2)$$

$$\frac{\partial T_2}{\partial t} = \frac{1}{\tau}(T_S - T_2), \quad (3)$$

in which L_f is the latent heat of fusion (definitions for all the other symbols are given in Tables 2 and 3). The first term on the right-hand side of (2) represents the forcing from radiative fluxes at the surface; the second term is for latent heat release due to freezing and melting of soil water and snow; and the last term, like the only term on the right-hand side of (3), is a ''restoring'' or relaxation term.

Because only one energy budget is evaluated over the soil portion of a model grid area in CMC's version of ISBA, the thermal coefficient C_T includes the effect of bare soil, vegetation, and snow;

$$C_T = \frac{1}{\dfrac{(1 - \text{veg})(1 - p_{\text{sng}})}{C_g} + \dfrac{\text{veg}(1 - p_{\text{snv}})}{C_v} + \dfrac{p_{\text{sn}}}{C_S}}, \tag{4}$$

where the contribution of ground, vegetation, and snow (i.e., C_g, C_v, and C_S) are weighted by the fraction of the model grid area covered by vegetation (veg) and snow (p_{sn}), and the fraction of bare soil and vegetation covered by snow (p_{sng} and p_{snv}). The thermal coefficient for vegetation (C_v) has fixed values of 1×10^{-5} or 2×10^{-5} K m^2 J^{-1} for high and low vegetation, respectively. For bare ground, the thermal coefficient is given by

$$C_g = C_{\text{gsat}}\left(\frac{w_{\text{sat}}}{w_2}\right)^{b/(2\ln 10)}, \qquad C_g \le 2 \times 10^{-5}\ \text{K m}^2\ \text{J}^{-1}, \tag{5}$$

in which w_{sat} (soil water content at saturation), C_{gsat} (value of C_g at saturation), and b (slope of the retention curve) are soil parameters that are determined from the soil texture (see Noilhan and Lacarrère 1995). Details concerning the snow coverage fraction and the snow thermal coefficient are given in Bélair et al. (2003).

A schematic of ISBA's water budget is given in Fig. 1. This diagram shows all the water reservoirs (w_g, w_2, w_F, W_r, W_S, and W_L) that are represented in ISBA, as well as all the sources (precipitation), sinks (runoff and drainage), and transfers between these reservoirs. In ISBA, the superficial and rooting-depth soil water contents both evolve according to the following force–restore equations:

TABLE 3. Important variables in ISBA.

Variable	Definition	Units
P_r	Rain rate	Kg m^{-2} s^{-1}
P_S	Snow rate	Kg m^{-2} s^{-1}
E_g	Bare soil evaporation	Kg m^{-2} s^{-1}
E_S	Snow sublimation rate	Kg m^{-2} s^{-1}
E_r	Direct evaporation from vegetation canopy	Kg m^{-2} s^{-1}
E_{tr}	Vegetation transpiration	Kg m^{-2} s^{-1}
C_T	Surface thermal coefficient	K m^2 J^{-1}
C_g	Bare soil thermal coefficient	K m^2 J^{-1}
C_S	Snow thermal coefficient	K m^2 J^{-1}
C_v	Vegetation thermal coefficient	K m^2 J^{-1}
veg	Fraction of model grid area covered by vegetation	
p_{sn}	Fraction of model grid area covered by snow	
p_{sng}	Fraction of bare soil covered by snow	
p_{snv}	Fraction of vegetation covered by snow	
freez_S	Freezing fluxes of snow	Kg m^{-2} s^{-1}
melt_S	Melting fluxes of snow	Kg m^{-2} s^{-1}
freez_g	Freezing fluxes of soil water	Kg m^{-2} s^{-1}
melt_g	Melting fluxes of soil water	Kg m^{-2} s^{-1}
R_{snow}	Snowmelt runoff	Kg m^{-2} s^{-1}
R_{surf}	Surface runoff	Kg m^{-2} s^{-1}
R_{veg}	Vegetation throughfall	Kg m^{-2} s^{-1}
drain	Deep soil drainage	Kg m^{-2} s^{-1}

$$\frac{\partial w_g}{\partial t} = C_1[(1 - \text{veg})(1 - p_{\text{sng}})P_r + (1 - p_{\text{snv}})R_{\text{veg}} + R_{\text{snow}} - E_g - R_{\text{surf}}] - \frac{C_2}{\tau}(w_g - w_{\text{geq}}), \tag{6}$$

$$\frac{\partial w_2}{\partial t} = \frac{1}{\rho_w d_2}[(1 - \text{veg})(1 - p_{\text{sng}})P_r + (1 - p_{\text{snv}})R_{\text{veg}} + R_{\text{snow}} + \text{melt}_g - \text{freez}_g - E_g - E_{\text{tr}} - R_{\text{surf}}] - \frac{C_3}{d_2\tau}\text{MAX}[0, (w_2 - w_{\text{fc}})], \tag{7}$$

where ρ_w is the liquid water density; d_2 is the rooting depth; w_{geq} is an equilibrium water content; w_{fc} is the soil water content at field capacity; and C_1, C_2, and C_3 are coefficients that depend on the soil texture (see Noilhan and Planton 1989; Mahfouf and Noilhan 1996).

The evolution equation (7) for w_2 represents the water budget over a soil layer of depth d_2. The first term on the right-hand side includes the effect of rainfall, vegetation and snowmelt runoff, melting/freezing of soil water, evaporation, and surface runoff. The other term, for drainage, is proportional to the water amount exceeding field capacity (i.e., $w_2 - w_{\text{fc}}$) (see Mahfouf and Noilhan 1996). Equation (6) for w_g is similar to (7) except for the melting/freezing and transpiration terms that are not included, and the restore term that is used for this layer. The subgrid-scale surface runoff R_{surf} that appears in the two equations is evaluated with the variable infiltration capacity scheme described in Wood et al. (1992), which is based on the so-called Nanjing model (see Zhao 1992).

Rainfall and dew intercepted by the canopy foliage feed a reservoir of water content, W_r. This water evaporates in the air at a potential rate from the fraction δ of the foliage covered with a film of water, as the remaining part $(1 - \delta)$ of the leaves transpires. Following Deardorff (1978),

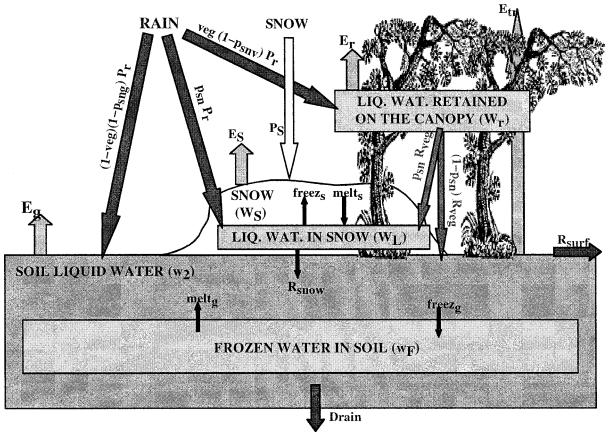

FIG. 1. Schematic diagram of the hydrological cycle represented in the modified version of ISBA. All the water reservoirs are shown, including new ones for liquid water retained in the snow pack and frozen water in the soil (see Bélair et al. 2003, for more details about these reservoirs). Exchange processes between all the reservoirs are also shown. All the symbols are explained in Tables 2 and 3.

$$\frac{\partial W_r}{\partial t} = \text{veg}P_r - (E_v - E_{\text{tr}}) - R_{\text{veg}}. \quad (8)$$

Vegetation throughfall R_{veg} occurs when W_r exceeds a maximum value W_{rmax} given by

$$W_{\text{rmax}} = 0.2\text{vegLAI}, \quad (9)$$

where LAI is the leaf area index.

The surface heat turbulent fluxes are calculated by means of classical aerodynamic equations, using a thermal drag coefficient from Delage and Girard (1992) and Delage (1997). Calculations for the sensible heat flux are straightforward, using the surface temperature T_S that evolves according to (2). The latent heat flux LE, on the other hand, is the sum of fluxes over bare ground, vegetation, and snow, weighted by the areas $(1 - \text{veg})(1 - p_{\text{sng}})$, $\text{veg}(1 - p_{\text{snv}})$, and p_{sn}, respectively. The details of surface fluxes calculations are given in Noilhan and Planton (1989).

4. The sequential assimilation of surface variables

To properly initialize ISBA's surface temperatures (T_S and T_2) and soil water contents (w_g and w_2), a sequential assimilation system was also operationally implemented at CMC. The basic idea behind this technique is to relate assimilation increments on soil moisture and surface temperature to model errors in low-level air temperature (T) and relative humidity (RH), following the linear equations

$$\begin{aligned}\delta w_g &= w_g^a - w_g^f \\ &= \alpha_1(T^o - T^f) + \alpha_2(\text{RH}^o - \text{RH}^f), \quad (10)\\ \delta w_2 &= w_2^a - w_2^f \\ &= \beta_1(T^o - T^f) + \beta_2(\text{RH}^o - \text{RH}^f), \quad (11)\end{aligned}$$

where the subscripts "a," "f," and "o" refer to "analyzed," "forecasted," and "observed."

Based on the work of Mahfouf (1991), who estimated the statistical distribution of the α_1, α_2, β_1, and β_2 coefficients at each local solar time using a Monte Carlo method, Bouttier et al. (1993a) proposed an analytical formulation of the coefficients in the form of continuous functions of surface characteristics, which was later modified by Giard and Bazile (2000). The parameters appearing in these continuous functions were calculated to fit to a large sample of α and β coefficients computed exactly using the Monte Carlo method (see Bouttier et al. 1993a). These coefficients are specified by linearly interpolating hourly tabulated values (not shown here) to the local solar time of each model grid point.

For the surface temperatures, the analysis increments are directly related to model errors at screen level, following

$$\delta T_S = T_S^a - T_S^f = T^o - T^f \quad \text{and} \quad (12)$$

$$\delta T_2 = T_2^a - T_2^f = \frac{(T^o - T^f)}{2\pi}. \quad (13)$$

To avoid performing the analysis in improper atmospheric and surface conditions, the analysis increments δT_S, δT_2, δw_g, and δw_2 are multiplied by a rejection factor rej, which depends on the conditions described in Table 4. Essentially, the surface assimilation has no impact in cloudy, rainy, snowy, and windy conditions because in these situations the low-level air characteristics are more influenced by atmospheric processes (e.g., advection, condensation, and evaporation) than by surface fluxes. Moreover, the assimilation increments are set to zero for frozen soils or snow-covered surfaces.

Figure 2 shows how the sequential surface assimilation was set up in CMC's short-range weather forecast system. The GEM regional atmospheric model is launched twice a day, at 0000 and 1200 UTC, for 48-h integrations. The upper-air initial conditions for GEM are obtained from 12-h "spinup" cycles, in which data are assimilated every 6 h using a three-dimensional variational data assimilation (3DVAR) technique (Laroche et al. 1999). For the surface analyses, the increments δT_S, δT_2, δw_g, and δw_2 are calculated every day using 18-h forecasts valid at 1800 UTC, that is, at maximum insolation time over North America, when the correlation between surface- and low-level air characteristics is the greatest. The model errors are obtained by comparing model predictions with analyses of low-level air temperature and humidity (i.e., analyses of surface observations with first-guess fields produced by the regional model forecasts). The surface increments are applied at 0000 UTC the next day for the regional spin up. The surface initial conditions for the 1200 UTC spin ups are directly taken from the 12-h integrations, starting at 0000 UTC.

Even though the basic principle of this soil moisture assimilation is the same as the so-called error feedback

TABLE 4. Sequential assimilation rejection factor.

Variable	Rejection factor
Water	If only water, then rej = 0
Snow	$\text{rej} = \text{rej}\max\left(1 - \frac{W_S}{W_{\text{srej}}}, 0\right)$, where W_{srej} is a critical rejection value for the snow water equivalent
Frozen soil	$\text{rej} = \text{rej}\max\left(1 - \frac{\text{freez}}{\text{freez}_{\text{rej}}}, 0\right)$, in which $\text{freez} = \frac{w_f}{(w_f + w_2)}$, and where $\text{freez}_{\text{rej}}$ is a critical rejection value for the fraction of frozen soil water content
Precipitation	$\text{rej} = \text{rej}\max\left(1 - \frac{\text{precip}_{\text{mod}}}{\text{precip}_{\text{rej}}}, 0\right)$, where $\text{precip}_{\text{mod}}$ is an avg value of predicted precipitation accumulation in the 12-h period centered on the analysis time, and $\text{precip}_{\text{rej}}$ is a critical rejection value for precipitation
Advective effects	$\text{rej} = \text{rej}\max\left(2 - \frac{\text{wind}_{\text{mod}}}{\text{wind}_{\text{rej}}}, 0\right)$, where wind_{mod} is the wind module and wind_{rej} is a critical rejection value for low-level wind
Clouds	$\text{rej} = \text{rej}\min\left(2\frac{\text{solar}_{\text{ground}}}{\text{solar}_{\text{top}}}, 1\right)$, where $\text{solar}_{\text{ground}}$ and $\text{solar}_{\text{top}}$ are the incident solar radiation fluxes at the surface and at the top of the atmosphere

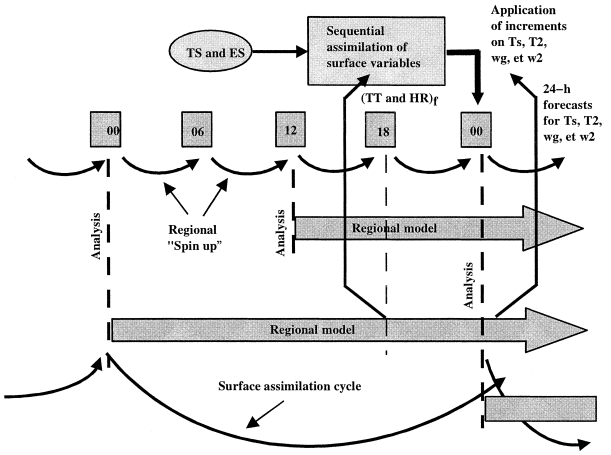

FIG. 2. Schematic diagram of the sequential assimilation of surface variables, TS and ES are analyses of 2-m air temperature and dewpoint temperature depression, that is, $T - T_d$, whereas TT and HR are forecasts (see subscript "f") of 2-m air temperature and relative humidity.

mechanism that was used in the previous operational system (see Mailhot et al. 1997), its application within the CMC's regional weather forecasting system is quite different. In the previous system, assimilation increments were applied to a single variable for soil moisture availability using errors on dewpoint depression. In the new system, these increments are evaluated from model errors in both air temperature and relative humidity, and are applied to both soil moisture and surface temperature variables (at two levels). Moreover, 5-day means of model errors were used in the previous operational system, whereas no such averaging is performed in the new system.

5. Summertime preimplementation tests

a. Experimental setup and ISBA's input data

Because root-zone soil water evolves very slowly, evaluation of the new surface modeling and assimilation system requires a reasonably long spinup period. Therefore, only the results obtained during the last month of a 4-month assimilation cycle, which started on 1 May 2000, were examined for this study (i.e., August 2000). Even though the new sequential assimilation described in the previous section accelerates the spinup process, it is not certain, a priori, that a 3-month period is sufficiently long to allow soil water to reach a true equilibrium state that would be independent of the initial conditions. Unfortunately, the computer cost associated with integrating the GEM regional forecasting system prevented us from running the surface assimilation cycle for a longer period to verify this hypothesis. The continuous real-time integration of the surface modeling and assimilation system that is now being run operationally at CMC will provide some answers concerning this question.

Figure 3 shows a few of the geophysical fields that are required to run the new surface modeling system. Vegetation and soil characteristics are spatially averaged in GEM's entry programs in order to provide the physics package with surface fields that are representative of the model grid areas associated with all the model grid points (see Noilhan and Lacarrère 1995). The source data for this averaging comes from several ancillary databases. Vegetation properties are obtained from a United States Geological Survey (USGS) database that covers North America at a resolution of about 1 km. For soil texture, a high-resolution (i.e., ~1 km) multilayer soil characteristics dataset based on the United States Department of Agriculture (USDA) State Soil Geographic Database (STATSGO) is used over the United States, whereas a lower-resolution database, from Agriculture Canada, is used over Canada.

Vegetation's main characteristics (e.g., leaf area index, vegetation fraction) vary according to the day of the year, following a preestablished table (similar to those shown in Giard and Bazile 2000). The upper panels in Fig. 3 show that most of North America is covered with relatively dense vegetation in August. For soil texture, the sand and clay percentages are calculated from the dominant soil type and are then used to determine

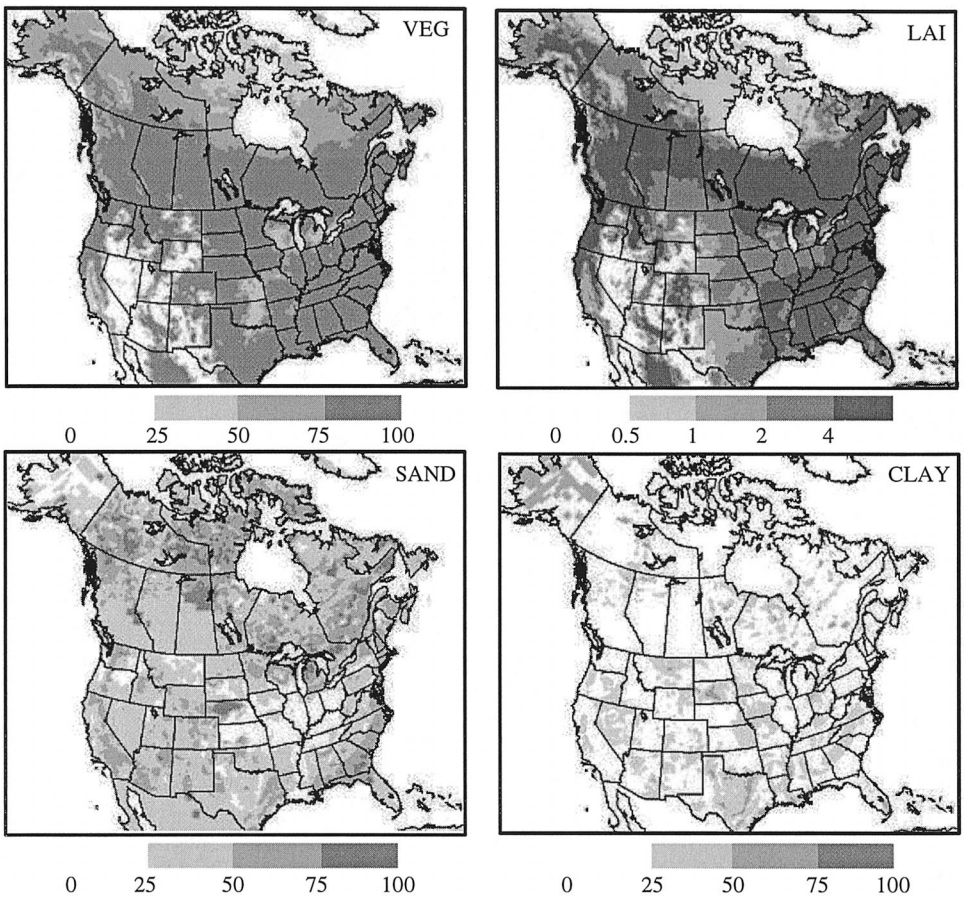

FIG. 3. Vegetation and soil characteristics for the central portion of the integration domain: (top) the vegetation fractional coverage (VEG; %) and leaf area index (LAI; $m^2\ m^{-2}$), valid for the model run initialized at 0000 UTC on 2 Aug 2000, and (bottom) the sand and clay content (%) of the soil.

the relevant parameters using relations from Noilhan and Lacarrère (1995). The lower panels of Fig. 3 show that soil texture varies greatly over North America. This figure also illustrates the difference in resolution between the two soil databases.

The surface prognostic variables for the first day of the 4-month assimilation cycle (i.e., 1 May 2000) are initialized in an arbitrary manner. The superficial surface temperature is specified directly from the 1.5-m-level air temperature analysis, whereas an average of the previous 5 days is used for the mean surface temperature. These surface temperature initial conditions are not of crucial importance because these variables adjust fairly rapidly (even the mean surface temperature) to radiative forcing.

Soil moisture, however, evolves more slowly (especially for the deep soil layer) and, thus, requires a more proper initialization in order to reduce its adjustment time. Unfortunately, no analysis was available for this quantity. Values halfway between the volumetric water contents at the wilting point and field capacity were used as initial conditions for both superficial and deep soil water for 1 May 2000. Diagnostics from the sequential assimilation during the first weeks of numerical integration revealed that predicted low-level air was in general too humid and too cold, which indicated that the soil was probably too moist. The model thus had, in these first weeks of integration, a tendency toward a drier equilibrium state, due to drying tendencies from the sequential assimilation and large surface evaporation.

Initial conditions for other surface variables, with much less impact on the long-term summertime evolution of the surface, also had to be specified for the first day of the assimilation cycle: the water retained in the vegetation canopy was set to zero, the snow depth was obtained from a CMC operational analysis (Brasnett 1999), the snow density and albedo were set to values typical of fresh snow, and the frozen soil water was set to zero everywhere except under the snowpack. All the surface prognostic variables were carried on without any changes from one 24-h integration to the next, except for the surface temperatures and soil moistures, which were modified by the surface sequential assimilation (see Fig. 2).

The rest of this section presents the diagnostics and

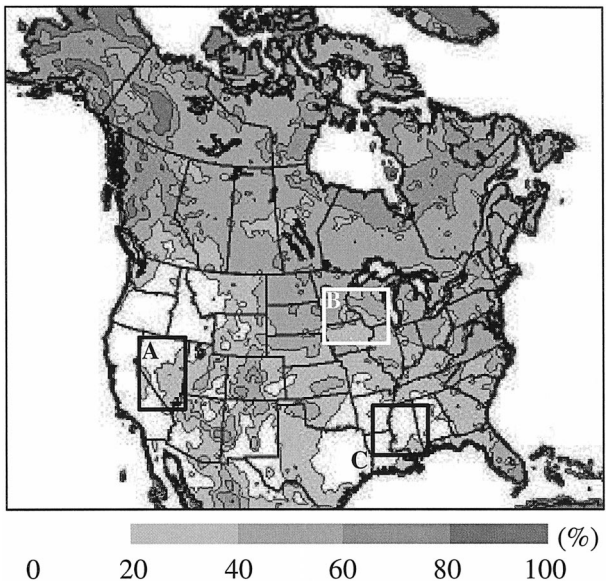

FIG. 4. Fraction (%) of days during Aug 2000 for which the sequential assimilation of surface variables was not activated, due to unfavorable atmospheric conditions. The three squares, identified by the letters ''A,'' ''B,'' and ''C,'' indicate the position of averaging domains used for the time series shown in Figs. 8, 9, and 10.

statistics related to the surface sequential assimilation cycle for August 2000, as well as the objective evaluations for this same period.

b. Sequential assimilation statistics

Initial conditions of surface temperature and soil moisture have a significant influence on surface fluxes and their partitioning into sensible and latent heat fluxes. It is therefore important to examine results and diagnostics from the surface sequential assimilation system before objectively evaluating the new surface modeling system.

Figure 4 shows the percentage of days during August 2000 for which the sequential assimilation of surface variables was not activated, due to unfavorable atmospheric conditions. As expected, this ''rejection'' fraction produced by the sequential assimilation corresponds well with monthly means of 12-h precipitation (centered on the time of assimilation, 1800 UTC) and the fraction of top-of-atmosphere solar radiation that reaches the surface at 1800 UTC (Fig. 5).

In general, the sequential assimilation is performed less often in the northern and eastern parts of the North American continent, due to more cloudy and rainy conditions. Over most of Canada and the eastern part of the continent, the rejection fraction is on the order of 40%–60%. This fraction is much lower for the western part of the United States, that is, less than 20%, where less rain and cloud activity was predicted and observed. One should note that except for a few regions, like Alaska, British Columbia, and the surrounding areas of Hudson Bay, the rejection fraction does not exceed 60%, which assures us that the sequential assimilation should be effective at least every other day, on average, for most of the model grid points in North America. Results discussed in the next section reveal that this assimilation frequency is sufficient to improve the numerical prediction of the boundary layer and precipitation, compared to the previous operational forecasting system.

1) MONTHLY MEAN MAPS

Figures 6 and 7 show maps for monthly averages of surface warming and soil moistening increments produced by the sequential assimilation in August 2000. These figures expose the tendency of the assimilation system to warm the surface and dry the soil over a large portion of North America, which is consistent with tendencies produced in the first 3 months of the assimilation cycle. It thus seems that soils are still too humid and that the surface has still not reached an equilibrium state, at least for a certain portion of the continent, that is independent of the chosen initial conditions.

The time necessary to adjust from incorrect initial conditions depends on atmospheric conditions, on surface types, and on the ''difference'' between the initial and adjusted soil moistures. For some regions, a period of several months should be expected before reaching an equilibrium state (see Douville et al. 2000). In the present case, the surface warming and soil drying shown in Figs. 6 and 7 are found to be larger for the western portion of the United States. The soils in this area are, in general, drier compared to the rest of the continent, because they are subjected to much less precipitation. Because soil drying mainly occurs through surface evaporation and assimilation adjustments (which could be very small for the deep-soil reservoir, as will be discussed below), the timescales associated with soil drying could be significantly longer than the timescales associated with soil moistening, which can occur fairly rapidly in regions having considerable summertime precipitation. Considering also that ''dry'' equilibrium states could be relatively far away, compared to the rest of the continent, from the initial conditions that were imposed at the beginning of the assimilation cycle (e.g., from halfway between the wilting point and field capacity, to values much lower than the wilting point), it is understandable that the time necessary to reach model equilibrium could be on the order of months for some regions (e.g., the southwestern part of the United States).

It is interesting to note that cooling and moistening tendencies are produced by the sequential assimilation for a narrow band along the western coast of the continent. This artificial effect is related to observations near the West Coast that are often more representative of cooler and moister maritime air that is advected inland by the eastward general circulation. In the low-level air temperature and humidity analysis process, these observations incorrectly influence a wider region

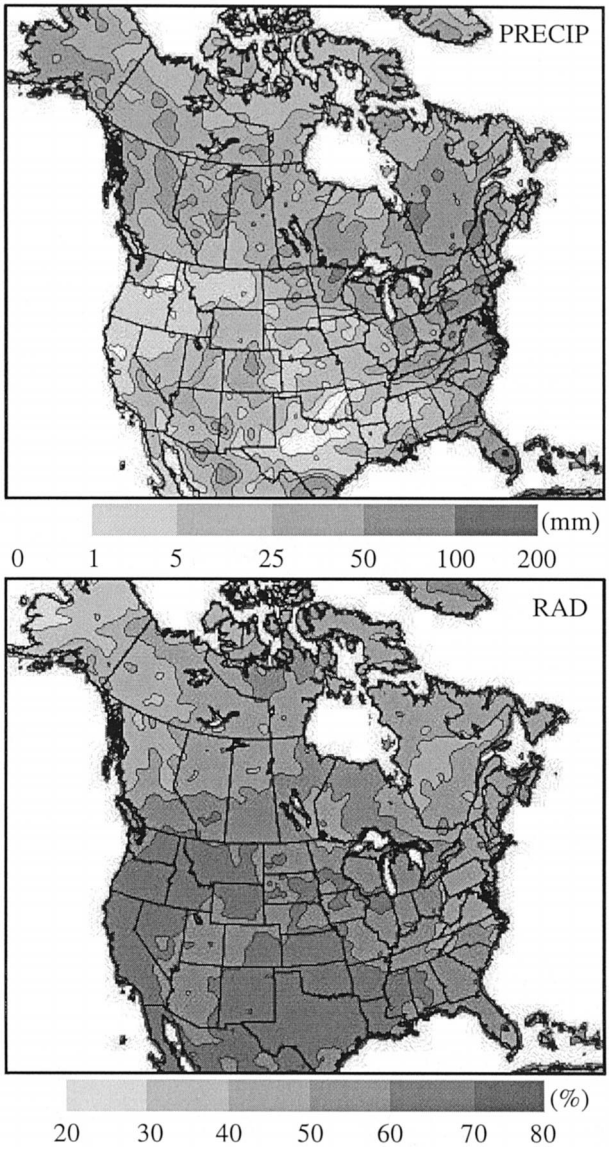

FIG. 5. Total precipitation and avg radiation for the 0000 UTC integrations of the parallel model during Aug 2000. (top) Accumulated 12–24-h precipitation (mm) and (bottom) avg fraction of solar radiation (%) reaching the surface (flux reaching the surface divided by the flux at the top of the atmosphere) at 18-h integration.

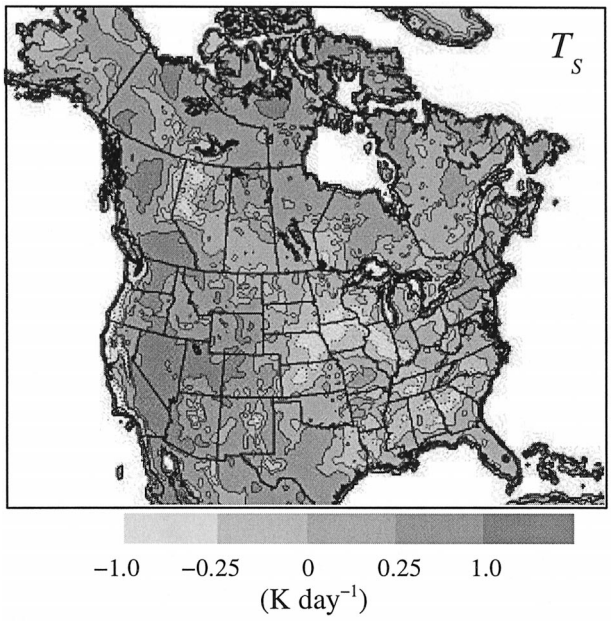

FIG. 6. Avg increments of surface temperature T_S (K day^{-1}) from the sequential assimilation of surface variables for Aug 2000. Full lines (dark shades) indicate warming increments, whereas dashed lines (pale shades) indicate cooling increments.

that reaches too far inland where, in reality, the advective effect of maritime air is not felt as much. Over these inland regions, the sequential analysis perceives the model prediction to be too warm and too dry. The resulting assimilation increments are thus to cool the surface and moisten the soil, which produces the narrow band along the West Coast seen in Figs. 6 and 7. This effect is not observed along the East Coast, where low-level air measurements are not influenced as much by maritime air due to the circulation, which is generally toward the ocean.

The assimilation increments presented in this section are not only due to incorrect low-level analyses or to the model spin up toward an equilibrium state; they are also related to model errors for the atmospheric forcing and/or the prognostic evolution of surface variables. It is possible, for instance, that low-level air temperature (or humidity) could be systematically underpredicted (or overpredicted) by GEM due to problems related to the numerical representation of the boundary layer, radiation, clouds, or precipitation (Bouttier et al. 1993b; Hu et al. 1999; Douville et al. 2000). It could also be that ISBA is not able to adequately represent surface processes even with ''perfect'' atmospheric forcing. As explained later, it is likely that this second factor is less important than the first. Unfortunately, the results shown in Figs. 6 and 7 do not allow us to quantify, or even identify, these potential errors.

2) TIME SERIES

To better understand the link between atmospheric conditions and the behavior of the sequential assimilation, Figs. 8, 9, and 10 show time series plots of spatially averaged forcing variables (over the small regions indicated in Fig. 4) and the response of the sequential assimilation.

The time series shown in Fig. 8 indicate that region A (i.e., Nevada; see Fig. 4) was mainly sunny and did not receive much precipitation during August 2000. Over this region, the temperature increments were positive each day of the month, indicating that all of the August 2000 18-h forecasts starting at 0000 UTC were

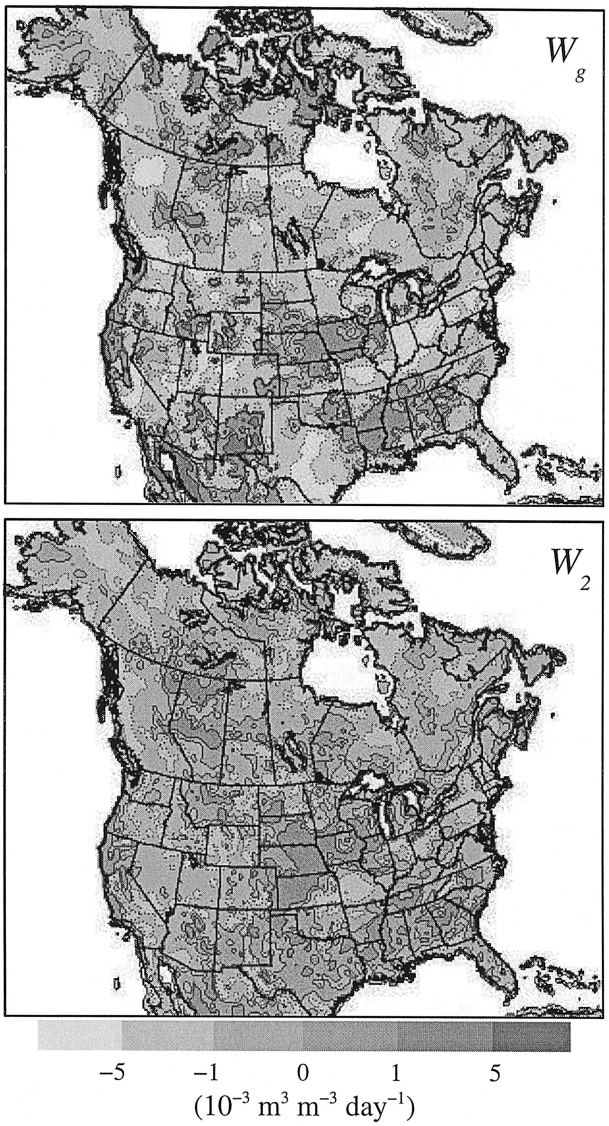

FIG. 7. Avg increments of soil moisture (m^3 m^{-3} day^{-1}) from the sequential assimilation of surface variables for Aug 2000. (top) The increments for the soil water content of the superficial reservoir w_g, and (bottom) the soil water content of the deep reservoir (w_2). Full lines (dark shades) indicate positive increments, whereas dashed lines (pale shades) indicate negative increments.

too cold over this region [see (12) and (13)]. In a consistent manner, the impact of the sequential assimilation was to dry the soil during this period, with larger increments for the superficial reservoir and almost no effect on the deep reservoir. This is in agreement with results presented in Bouttier et al. (1993b) who showed that the sequential assimilation mostly influences the superficial layer for regions with almost no vegetation. Because of this absence of deep reservoir drying by the sequential assimilation, soil drying over region A mainly occurs through surface evaporation, which could explain why the adjustment time toward an equilibrium state is so long.

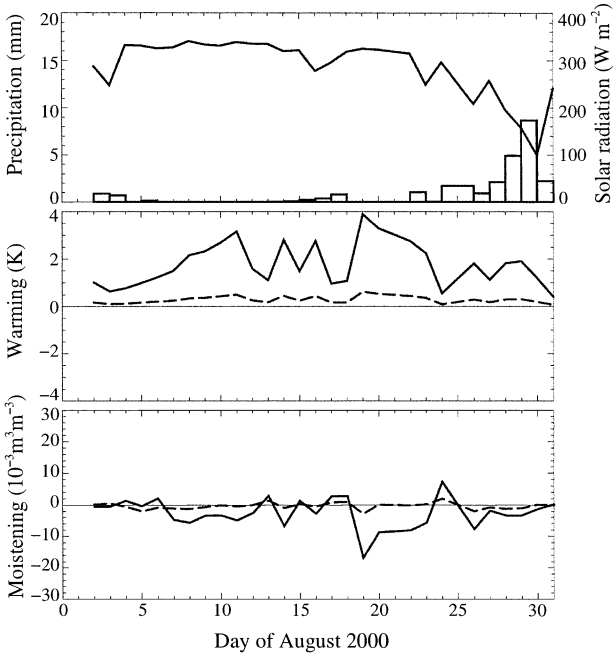

FIG. 8. Time series of forcing variables (i.e., solar radiation and accumulated precipitation) and of the sequential assimilation response (surface warming and soil moistening) spatially averaged over region A shown in Fig. 4 for each day during Aug 2000. (top) Daily averaged solar radiation at the surface (full line) is shown with daily precipitation (bars). (middle) The warming and (bottom) moistening tendencies applied at 0000 UTC of each day are shown for ISBA's two surface and soil levels (full and dashed lines are for the superficial and deep levels, respectively).

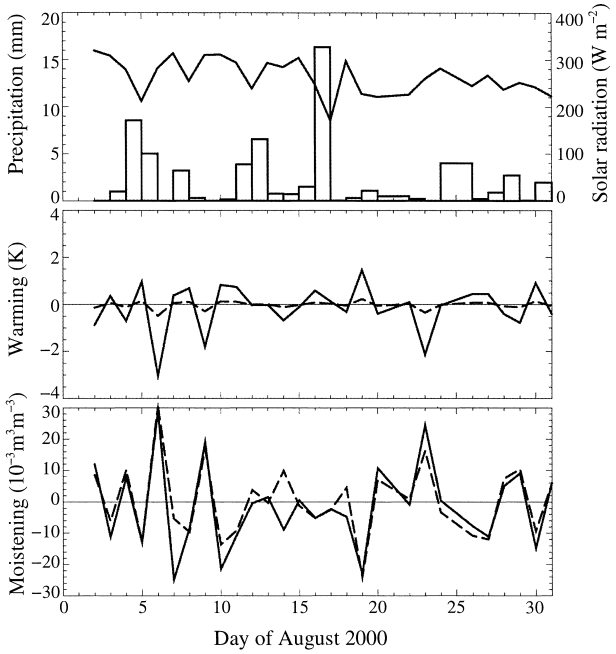

FIG. 9. Same as Fig. 8, but for region B indicated in Fig. 4.

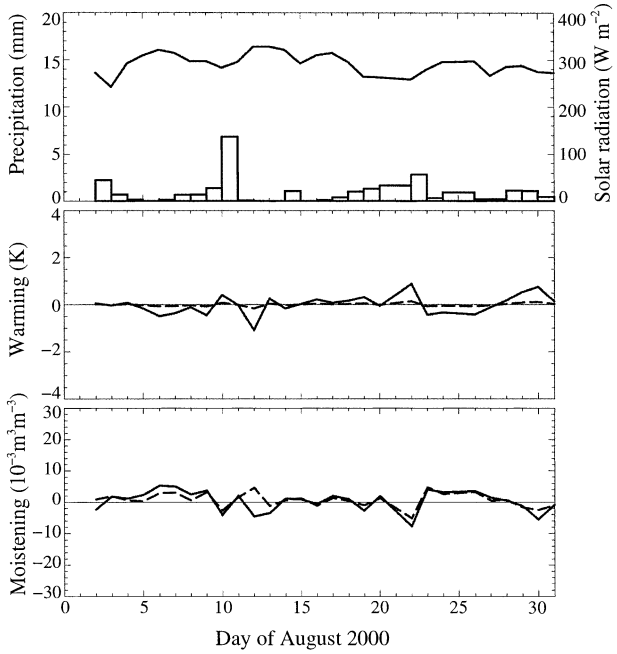

FIG. 10. Same as Fig. 8, but for region C indicated in Fig. 4.

Results over region B, which includes Wisconsin, Iowa, and Minnesota (see Fig. 4), are quite different (see Fig. 9). One should first note that several significant precipitation events were predicted for this region and that soil moisture increments from the sequential assimilation are large compared to those for region A. As was the case for region A, the increments on surface temperatures and soil water contents were negatively correlated, that is, cooling with moistening and vice versa. Because of the presence of vegetation over region B, which increases the correlations between deep soil moisture and surface air characteristics, the assimilation increments on the deep soil water content were as large as the increments on the superficial soil water. The two increments are in fact quite similar during August 2000, except for a few days (i.e., 14 and 18 August) when the increments were of different signs.

It is difficult from Fig. 9 to establish a clear link between precipitation and subsequent corrections from the sequential assimilation. For example, there is cooling and moistening after the precipitation event that occurred on 4–5 August, and the opposite for the precipitation event that occurred on 16–17 August. This type of behavior is expected, because it is quite likely that the atmospheric model could overpredict precipitation on one occasion, and underpredict it on another (same for radiative forcing).

It is clear, though, that analysis increments change sign more often for region B, as compared to region A (cf. Figs. 8 and 9). This indicates that model errors, either associated with the numerical representation of atmospheric forcing or of surface processes, are larger than the more systematic errors associated with a dry-down adjustment process for region B. Considering the very difficult nature of the parameterization of condensation processes in atmospheric models (see Frank 1983; Molinari and Dudek 1992; Bélair and Mailhot 2001) and the already proven ability of ISBA to correctly represent surface processes in stand-alone experiments over a wide range of surface types (Jacquemin and Noilhan 1990; Mahfouf 1990; Habets et al. 1999; Calvet et al. 1999), we believe it is more likely that the surface flux errors that lead to the corrections shown in Fig. 8 are more related to an incorrect representation of atmospheric forcing (precipitation and/or radiation) than to an incorrect representation of surface processes.

The third area under study, that is, region C (Mississippi; see Fig. 4), was less influenced by the sequential assimilation compared to the other two regions because the surface temperature and soil moisture increments are relatively small and centered around zero (see Fig. 10). This weaker effect of the sequential assimilation can be attributed to smaller model errors associated with the less numerous and weaker precipitation events that occurred over this region in August 2000 (as compared to region B), to a better partitioning of the assimilation increments between the superficial and deep soil water reservoirs due to the presence of vegetation (as compared to region A), and to a moister equilibrium state that was closer to the initial conditions.

It can thus be concluded from the time series shown in Figs. 8–10 that the role and impact of the surface sequential assimilation greatly depends on the region. For areas with less meteorological activity, like clouds and precipitation, errors associated with surface processes should dominate other errors that would be associated with atmospheric forcing. This was the case for region A where the errors were associated with a dry-down adjustment from incorrect initial conditions for soil moisture. For other regions (like regions B and C) where the frequency and intensity of precipitation events are larger, errors in the representation of surface processes should be small compared to those associated with precipitation and radiation. The role of the sequential assimilation is to correct, after the fact, these errors on atmospheric forcing. Time series such as those presented in this study are a useful tool to monitor the activity level of the sequential assimilation for certain key regions.

c. Objective evaluation

In the present investigation, we examined how the inclusion of ISBA translated into improved meteorological predictions, like surface air characteristics (temperature and humidity) and precipitation. The objective evaluations presented below were computed using the standard synoptic networks of surface stations and radiosondes (not shown). It should be mentioned that a large portion of the surface stations are located in the eastern part of North America, with fewer stations in

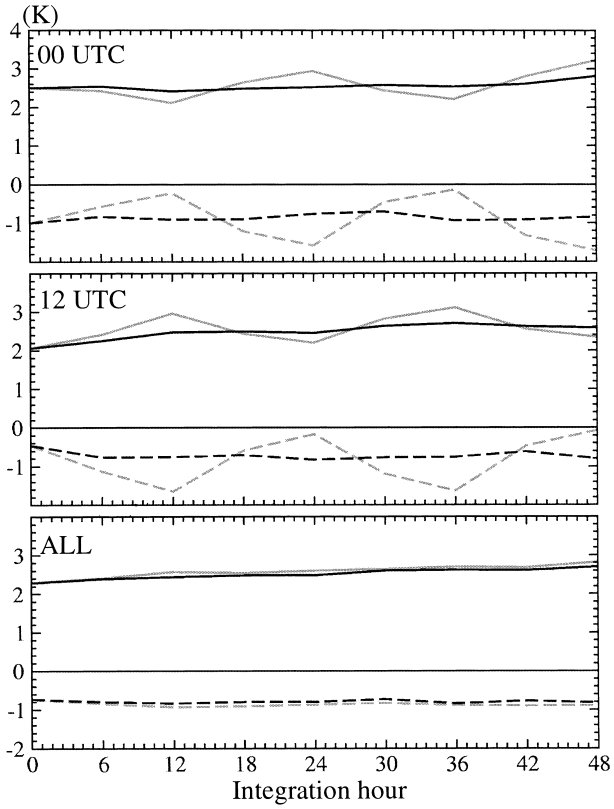

FIG. 11. Objective evaluation of model surface temperature against observations. The rms errors are represented by the full lines whereas the biases are shown by the dashed lines. Scores for the operational and ISBA versions of the model are indicated by the gray and black lines, respectively. The top two panels show the scores for the forecasts initialized at 0000 and 1200 UTC, while the results in the bottom panel include all the forecasts.

mountainous regions in the west. Surface stations for which the altitude was too different from the associated model gridpoint height were not considered in the calculations. The upper-air (i.e., radiosondes) observational network is considerably less dense than the surface station network, but provides a more even spatial coverage over the North American continent.

1) NEAR-SURFACE AIR CHARACTERISTICS

Figure 11 shows the root-mean-square (rms) and bias errors for the screen-level temperature for both ISBA and the simple force–restore scheme that was used in the previous CMC's operational regional weather forecast model. It is interesting to note that improvement of surface air temperature associated with the inclusion of the new surface modeling system seems marginal when looking at the combination of forecasts from 0000 and 1200 UTC (lower panel of Fig. 11). Examined separately, however, results from runs starting at 0000 and 1200 UTC reveal that the new surface system significantly improves the diurnal cycle's amplitude, which is significantly underestimated with the previous force–restore scheme. For the two upper panels of Fig. 11, the temperature bias scores of the previous operational system show that this model is relatively colder around 0000 UTC (evening), and vice versa at 1200 UTC (early morning). In contrast, the bias and rms lines for the new system are almost flat, indicating that the amplitude of the diurnal cycle is better represented. Because the model has, on average, a cold bias, the new system's errors are smaller in the evening and larger in the morning, as compared to the previous operational system. The origin of this cold bias is currently under investigation.

The monthly averaged surface air temperature differences between 0000 and 1200 UTC reveal, in another way, the positive impact of the new surface system on the predicted amplitude of the diurnal cycle. Figure 12 shows that the new surface modeling system is able to forecast temperature differences greater than 16 K over the western United States (e.g., Oregon, Idaho, Nevada, and California) that compare well with the analyzed temperature differences. In contrast, the temperature differences produced by the previous operational model are considerably less over the same region (i.e., <12 K). It is worth noting that other studies describing the use of new surface modeling systems do not report on such remarkable improvements in the representation of the temperature diurnal cycle's amplitude (e.g., Giard and Bazile 2000).

Objective evaluation of the screen-level humidity for the two surface systems is shown in Fig. 13. For historical reasons, these humidity scores are computed at CMC using dewpoint depression (i.e., $T - T_d$), which has the undesirable consequence that temperature and humidity scores are not independent.

It is evident from Fig. 13 that the previous operational model also produces a diurnal oscillation in both rms and bias scores for dewpoint depression. It is difficult, though, to determine whether this effect is entirely due to the underestimation of the temperature diurnal cycle's amplitude (Fig. 11), or if it is also partly caused by dewpoint temperature errors. As was the case for temperature, the oscillations in dewpoint depression are significantly reduced with the new surface system. Again, it is difficult to separate the contributions from humidity and temperature for this improvement. For rms errors, the new system also produces diurnal oscillations, which indicate that the new model, as was the case for the previous operational model, produces larger low-level humidity errors at 0000 UTC, as compared to 1200 UTC. The near-surface relative humidity at 0000 UTC does not only depend on surface fluxes, but also on the daytime evolution of the well-mixed layer. It is thus possible that the increased errors in dewpoint depression at this time of the day could be partly caused by an incorrect representation of the daytime convective boundary layer.

It is also interesting to note from Fig. 13 that the sign of the humidity bias is different for the two model configurations. Forecasts from the previous operational sys-

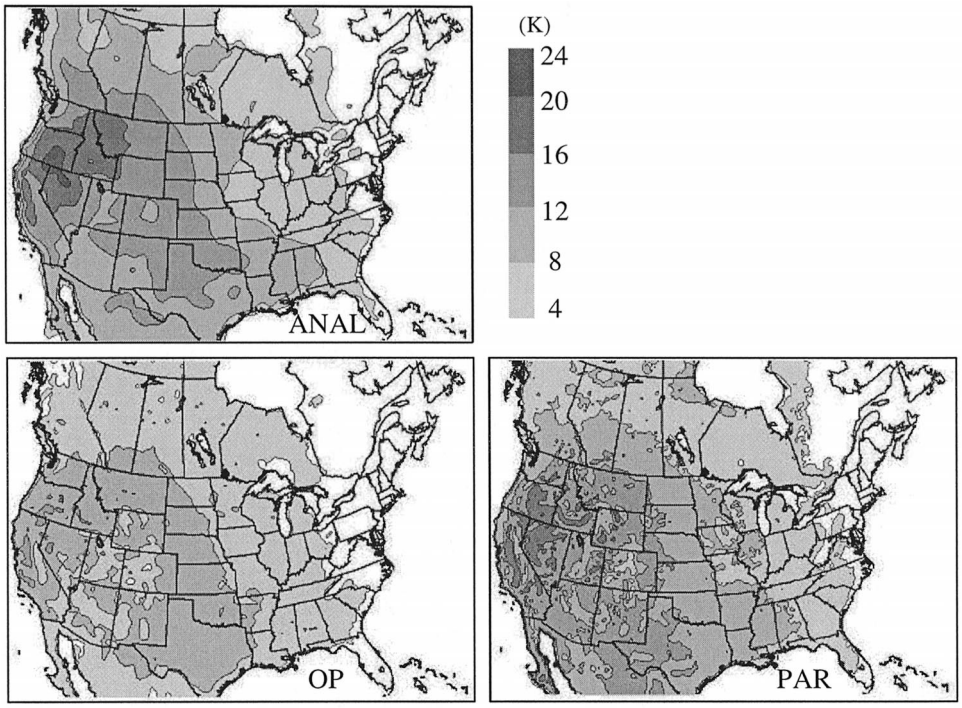

FIG. 12. Differences of screen-level air temperature (K) between 0000 and 1200 UTC from the regional model analyses (based on data assimilation using the regional atmospheric model forecast as a first guess) (ANAL), the operational runs (OP), and the parallel runs, including ISBA (PAR), averaged for the month of August 2000.

tem are generally too humid at low levels, and the opposite is found for the model with ISBA (note though that the humidity bias is smaller with the new system). Because the temperature biases are very similar for the two systems (see Fig. 11), this difference of sign for the relative humidity bias seems to be related to surface evaporation.

This hypothesis is confirmed by results given in Fig. 14, which shows monthly averages of predicted sensible and latent heat fluxes from the two forecast systems. From this figure, it is clear that the Bowen ratio is quite different for the two surface modeling systems. With the new system, sensible heat fluxes are larger (by about 35% in the afternoon) than those from the previous operational model, and vice versa for latent heat fluxes. It is also interesting to note that evaporation is also reduced (by half) during nighttime hours (not the case for sensible heat fluxes), which suggests that nocturnal ground heat fluxes (or heat storage rate $G = R_n - H - \mathrm{LE}$) must be larger in the ISBA version, because the surface is generally cooler at night with this model version (i.e., larger net radiation).

2) ATMOSPHERIC BOUNDARY LAYER

Figures 15 and 16 show how these improvements on the prediction of screen-level temperature and humidity extend to the low- and midtroposphere. These two figures reveal that the new representation of surface fluxes leads to important reductions, for a layer reaching as high as 700 hPa, of cold and humid biases that existed in the previous operational model. The main effect of the new surface system is to shift bias curves to the right, without changing much of their vertical structure. Although reduced, there are still cold and humid biases in the boundary layer with the new system, even though biases near the surface are smaller or even of a different sign (for humidity). In these conditions, the sequential assimilation is not able to further reduce biases in the boundary layer, because screen-level results are too cold and too dry, leading to soil moisture increments of opposite signs (see section 4). The difference between the biases, near the surface and higher up in the atmosphere, suggests that there may be some problems with the representation of vertical transport of heat and humidity associated with boundary layer turbulence. It is also possible that an assimilation strategy that would include the boundary layer could lead to smaller biases in this part of the troposphere.

It is also encouraging to see in Figs. 15 and 16 that rms errors are also reduced with the new model. This improvement is particularly important for temperature. It is unclear, though, what portion of this rms error reduction is due to a decrease of the biases.

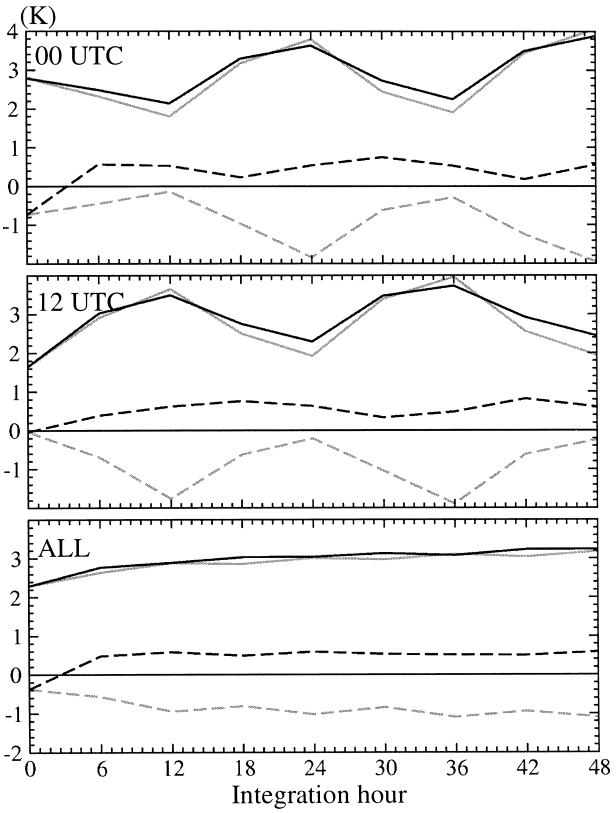

FIG. 13. Same as Fig. 11, but for the objective evaluation of model surface dewpoint depression (i.e., $T - T_d$).

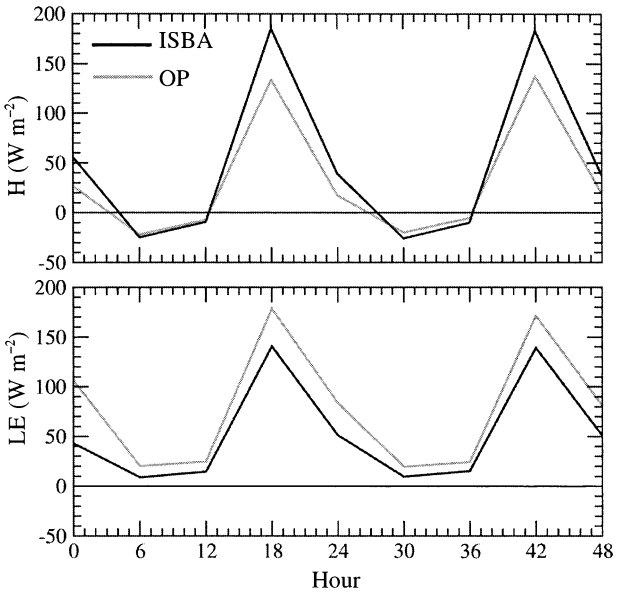

FIG. 14. Time series of (top) sensible and (bottom) latent heat fluxes averaged over North America at 6-h intervals for all the model integrations starting at 0000 UTC during Aug 2000. Surface fluxes from the operational and ISBA versions are represented by gray and black lines, respectively.

3) PRECIPITATION

With such important changes to the boundary layer temperature and humidity, the introduction of the new surface modeling system should be expected to significantly modify quantitative precipitation forecasts. Figures 17 and 18 show bias and threat scores, which are often used to objectively evaluate precipitation forecasts at operational centers (e.g., see Bélair et al. 2000). This verification is done using the synoptic observational network that covers North America. In the first 24 h of integration (Fig. 17), bias and threat scores are almost identical for the two model configurations. Essentially, the bias curves indicate that the regional forecast model tends to overpredict the number of events with weak precipitation, and show the reverse for events with more intense precipitation. This type of results for precipitation is expected for this particular model (see Bélair et al. 2000).

Objective scores for subsequent periods in the integrations, that is, 12–36 (not shown) and 24–48 h (see Fig. 18), reveal that the precipitation bias of the previous operational model increases with time. This tendency of the Canadian regional forecast model, which is well documented and was observed for many years, was often hypothesized to be related to an overestimated moistening of the boundary layer. It seems that the more realistic surface fluxes produced by the new surface system, which lead to a warmer and drier boundary layer, may have eliminated this increase of precipitation with time (cf. Figs. 17 and 18).

This positive result is an excellent example of the impact that surface fluxes may have on the evolution of weather systems, even for short-range weather prediction. Essentially, the partitioning of surface fluxes into sensible and latent heat components greatly influences the structure of the boundary or well-mixed layer (temperature, humidity, and lifting condensation level), which modulates the frequency and intensity of precipitation events, either convective or stratiform (see Betts and Ball 1998; Eltahir 1998; Pal and Eltahir 2001). In the present study, the larger Bowen ratio in the new model configuration leads to a warmer (see Fig. 15) and drier (see Fig. 16) boundary layer, which produces less precipitation than the previous operational model. Such an impact of surface fluxes on precipitation is in agreement with several other studies, including Clark and Arritt (1995) and Gallus and Segal (2000).

6. Summary and conclusions

This study describes the summertime improvement resulting from the operational implementation of a new surface assimilation and modeling system into the Canadian regional weather forecasting system. In this new system, surface processes over land are evaluated using the ISBA land surface scheme. Surface variables, including soil moisture, are initialized using a sequential assimilation technique in which model errors in low-

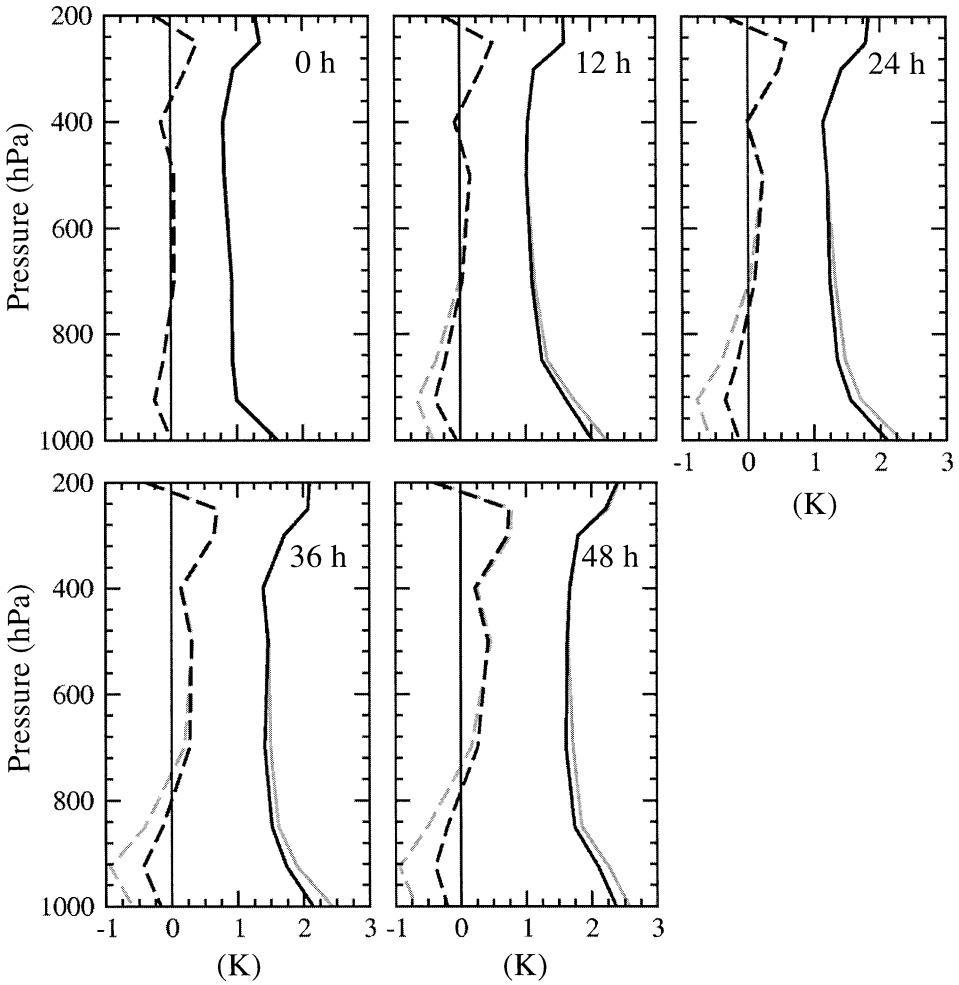

FIG. 15. Objective evaluation of upper-air temperature for 18 cases of Aug 2000. Rms (K, full lines) and bias (K, dashed lines) errors are shown for 0-, 12-, 24-, 36-, and 48-h forecasts from the operational (gray lines) and parallel (black lines) cycles.

level air temperature and relative humidity are used to determine assimilation increments on surface variables.

Diagnostics from the sequential assimilation cycle reveal that the magnitude and nature of the corrections applied to the surface variables depend on the surface and meteorological conditions observed over a particular region. For regions with weak meteorological activity (i.e., no clouds and precipitation), model errors in low-level air characteristics are more likely to be related to an incorrect representation of surface processes due to either erroneous initial conditions or inaccurate parameterizations in the land surface scheme. This type of situation was found over desert regions of the American Southwest, where the role of the surface assimilation was mainly to dry the upper portion of the soil in response to a dry-down adjustment caused by too-humid soil conditions at the beginning of the assimilation cycle.

In other regions characterized by a higher frequency and greater intensity of clouds and precipitation events, surface corrections were mainly associated with inaccurate atmospheric forcing. Those regions have reached an equilibrium state, which is independent of the surface conditions that were arbitrarily imposed at the start of the 4-month assimilation cycle. If we accept that, for those regions, errors in the atmospheric forcing are much larger than the errors associated with the representation of surface processes, it could be possible, in principle, to use diagnostics from the surface sequential assimilation to objectively evaluate the quality of the surface forcing provided by the atmospheric model (i.e., downwelling radiation and precipitation). The atmospheric forcing ''errors'' diagnosed by the surface assimilation system could be compared with actual model errors, using available precipitation and surface radiation observations. An evaluation technique based on this principle may be difficult to construct and other strategies, like the use of river flow observations through

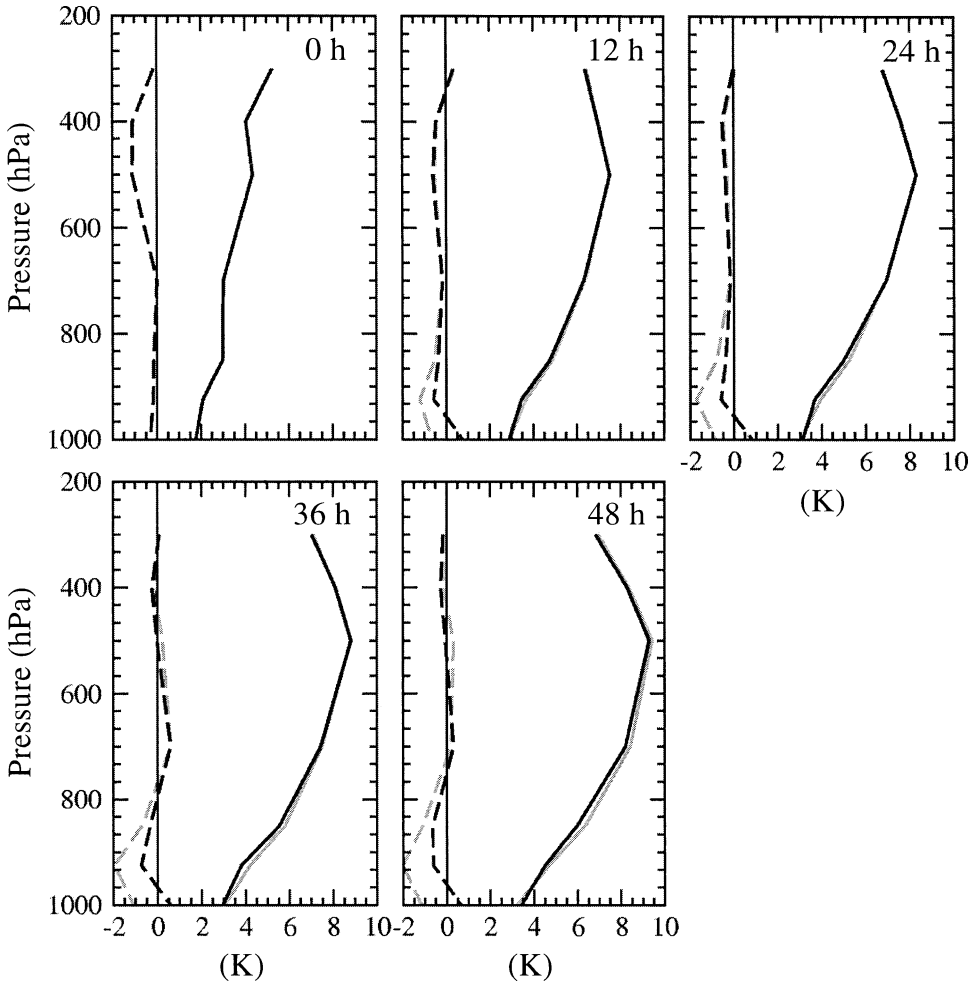

FIG. 16. Same as Fig. 15, but for dewpoint depression (i.e., $T - T_d$).

coupling of atmospheric and hydrological models, could be more promising. But we believe this idea deserves further attention.

Objective evaluation against observations from radiosondes and surface stations shows how the new surface modeling system improves the numerical prediction of summertime weather. It was first shown that the amplitude of the diurnal cycle of near-surface air temperature and humidity is larger with the new surface system, in better agreement with observations. (This increased amplitude of the diurnal cycle is related to significantly larger Bowen ratios with the new system.) This type of improvement was found to extend higher up in the troposphere (up to 700 hPa) where cold and humid biases were significantly reduced by introducing the new surface system.

However, the vertical structure of the temperature and dewpoint depression did not change significantly. Because these biases are not constant with height in the boundary layer, the near-surface biases are not representative of the rest of the boundary layer. Near-surface results indeed indicate cold and dry biases that represent the new surface equilibrium state, that is, these biases lead to soil moisture corrections of opposite signs. This type of bias structure in the boundary layer indicates that the treatment of vertical transport of heat and moisture associated with turbulence may need to be revised.

As expected from the boundary layer results, model precipitation was also found to be significantly influenced by the new representation of surface fluxes. The problematic increase (with integration time) of precipitation's positive bias was found to be significantly reduced with the new system, due to the warmer and drier boundary layer. This sensitivity of precipitation to surface fluxes shows the importance of correctly representing them in atmospheric models, even for short-range weather forecasting.

A similar surface assimilation and modeling system is currently being tested in CMC's global medium-range weather forecast suite. Other efforts are also underway concerning the representation of surface–air exchanges in CMC's atmospheric models. For instance, several modifications to ISBA are now being considered (e.g., better treatment of vegetation, surface emissivity, and

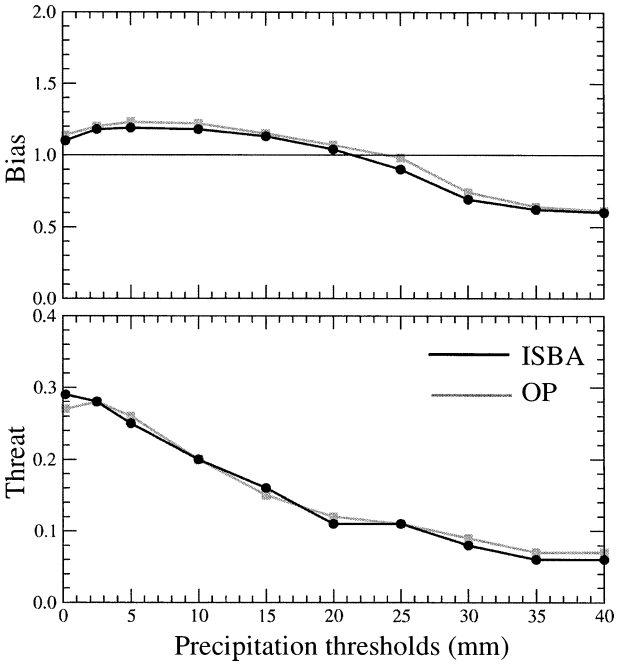

FIG. 17. (top) Bias and (bottom) threat scores for 0–24-h precipitation for 18 cases chosen during Aug 2000. The same proportion of cases initialized at 0000 and 1200 UTC was used. The gray lines with squares are for the operational runs. The black lines with circles are for the parallel runs with ISBA.

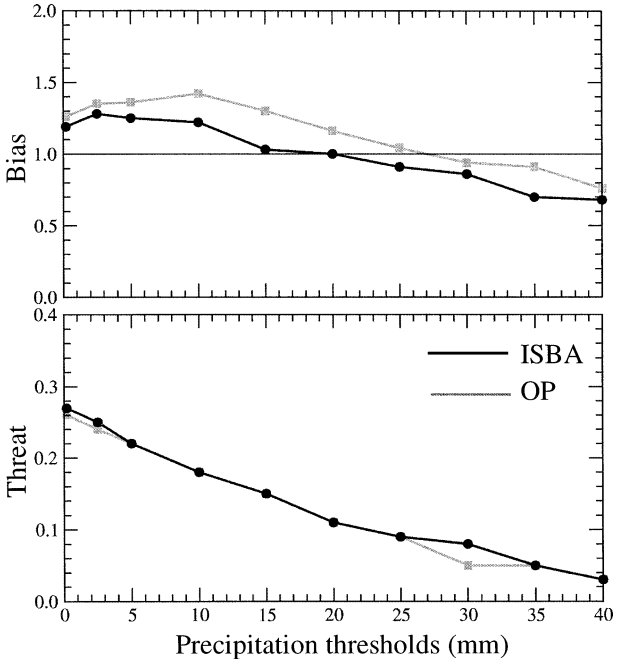

FIG. 18. Same as Fig. 17, but for 24–48-h precipitation.

a multilayer version). We are also planning on better specification of surface characteristics by using higher-resolution ancillary databases for vegetation and soil texture and by including near-real-time remote sensing (satellite) data for the leaf area index.

A new prototype of the surface assimilation and modeling system is now being examined. This new system would be based on offline integrations (i.e., outside the atmospheric model) of the land surface scheme, which would be driven by our best estimate of atmospheric forcing (temperature, humidity, wind, downwelling radiation, and precipitation), and in which various data [i.e., surface observations, Geostationary Operational Environmental Satellite (GOES) brightness temperatures, microwave radiances] would be assimilated using a four-dimensional assimilation scheme.

Acknowledgments. We would like to thank all those who were involved in the operational implementation of the new surface modeling and assimilation system at CMC. In the CMC development group, Louis Lefaivre, Gilles Verner, Judy St-James, and Normand Brunet greatly contributed to this implementation. In the CMC operation group, Garry Toth gave us a clearer view of the new system's impact on summertime weather forecasting. We are thankful to Peter Schut and Brian Monette from Agriculture Canada for providing soil texture data over Canada. We also appreciate the contribution of Ross Brown, our colleague from the Meteorological Research Branch of the Meteorological Service of Canada, who helped improve the final version of the text. Finally, this work greatly benefited from the interactions of the first author with Dr. Joël Noilhan, Dr. Florence Habets, Dominique Giard, and Eric Bazile of Météo-France.

REFERENCES

Bélair, S., and J. Mailhot, 2001: Impact of horizontal resolution on the numerical simulation of a midlatitude squall line: Role of implicit and explicit condensation. *Mon. Wea. Rev.,* **129,** 2362–2376.

——, A. Méthot, J. Mailhot, B. Bilodeau, A. Patoine, G. Pellerin, and J. Côté, 2000: Operational implementation of the Fritsch–Chappell convective scheme in the 24-km Canadian regional model. *Wea. Forecasting,* **15,** 257–274.

——, R. Brown, J. Mailhot, B. Bilodeau, and L.-P. Crevier, 2003: Operational implementation of the ISBA land surface scheme in the Canadian regional weather forecast model. Part II: Cold season results. *J. Hydrometeor.,* **4,** 371–386.

Beljaars, A. C. M., P. Viterbo, M. J. Miller, and A. K. Betts, 1996: The anomalous rainfall over the United States during July 1993: Sensitivity to land surface parameterization and soil moisture anomalies. *Mon. Wea. Rev.,* **124,** 362–383.

Benoit, R., J. Côté, and J. Mailhot, 1989: Inclusion of a TKE boundary layer parameterization in the Canadian regional finite-element model. *Mon. Wea. Rev.,* **117,** 1726–1750.

Betts, A. K., and J. H. Ball, 1998: FIFE surface climate and site-average dataset 1987–89. *J. Atmos. Sci.,* **55,** 1091–1108.

Bhumralkar, C. M., 1975: Numerical experiments on the computation of ground surface temperature in an atmospheric general circulation model. *J. Appl. Meteor.,* **14,** 67–100.

Boone, A., J.-C. Calvet, and J. Noilhan, 1999: Inclusion of a third soil layer in a land surface scheme using the force–restore method. *J. Appl. Meteor.,* **38,** 1611–1630.

——, V. Masson, T. Meyers, and J. Noilhan, 2000: The influence of

the inclusion of soil freezing on simulations by a soil–vegetation–atmosphere transfer scheme. *J. Appl. Meteor.,* **39,** 1544–1569.

Bouttier, F., J.-F. Mahfouf, and J. Noilhan, 1993a: Sequential assimilation of soil moisture from atmospheric low-level parameters. Part I: Sensitivity and calibration studies. *J. Appl. Meteor.*, **32,** 1335–1351.

——, ——, and ——, 1993b: Sequential assimilation of soil moisture from atmospheric low-level parameters. Part II: Implementation in a mesoscale model. *J. Appl. Meteor.,* **32,** 1352–1364.

Brasnett, B., 1999: A global analysis of snow depth for numerical weather prediction. *J. Appl. Meteor.*, **38,** 726–740.

Braud, I., J. Noilhan, P. Bessemoulin, P. Mascart, R. Haverkamp, and M. Vauclin, 1993: Bareground surface heat and water exchanges under dry conditions. *Bound.-Layer Meteor.,* **66,** 173–200.

Callies, U., A. Rhodin, and D. P. Eppel, 1998: A case study on variational soil humidity analysis from atmospheric observations. *J. Hydrol.*, **212–213,** 95–108.

Calvet, J.-C., and Coauthors, 1999: MUREX: A land-surface field experiment to study the annual cycle of the energy and water budgets. *Ann. Geophys.,* **17,** 838–854.

Chang, J.-T., and P. J. Wetzel, 1991: Effects of spatial variations of soil moisture and vegetation on the evolution of a prestorm environment: A numerical case study. *Mon. Wea. Rev.*, **119,** 1368–1390.

Charney, J. G., W. J. Quirks, S. H. Chow, and J. Kornfield, 1977: A comparative study of the effects of albedo change on drought in semi-arid regions. *J. Atmos. Sci.*, **34,** 1366–1385.

Chen, F., and Coauthors, 1996: Modeling of land surface evaporation by four schemes and comparison with FIFE observations. *J. Geophys. Res.*, **101,** 7251–7268.

Chen, T. H., and Coauthors, 1997: Cabauw experimental results from the Project for Intercomparison of Land-Surface Parameterization Schemes. *J. Climate,* **10,** 1194–1215.

Chouinard, C., J. Mailhot, H. L. Mitchell, A. Staniforth, and R. Hogue, 1994: The Canadian regional data assimilation system: Operational and research applications. *Mon. Wea. Rev.*, **122,** 1306–1325.

Clark, C. A., and R. W. Arritt, 1995: Numerical simulations of the effect of soil moisture and vegetation cover on the development of deep convection. *J. Appl. Meteor.*, **34,** 2029–2045.

Côté, J., M. Roch, A. Staniforth, and L. Fillion, 1993: A variable-resolution semi-Lagrangian finite-element global model of the shallow-water equations. *Mon. Wea. Rev.*, **121,** 231–243.

——, J. G. Desmarais, S. Gravel, A. Méthot, A. Patoine, M. Roch, and A. Staniforth, 1998a: The operational CMC–MRB global environmental multiscale (GEM) model. Part II: Results. *Mon. Wea. Rev.*, **126,** 1397–1418.

——, S. Gravel, A. Méthot, A. Patoine, M. Roch, and A. Staniforth, 1998b: The operational CMC–MRB global environmental multiscale (GEM) model. Part I: Design considerations and formulation. *Mon. Wea. Rev.*, **126,** 1373–1395.

Courtier, P., J. N. Thépaut, and A. Hollingsworth, 1994: A strategy for operational implementation of 4Dvar using an incremental approach. *Quart. J. Roy. Meteor. Soc.,* **120,** 1367–1387.

Deardorff, J. W., 1978: Efficient prediction of ground surface temperature and moisture with inclusion of a layer of vegetation. *J. Geophys. Res.*, **83,** 1889–1903.

Delage, Y., 1997: Parameterising sub-grid scale vertical transport in atmospheric models under statically stable conditions. *Bound.-Layer Meteor.,* **82,** 23–48.

——, and C. Girard, 1992: Stability functions correct at the free convection limit and consistent for both the surface and Ekman layers. *Bound.-Layer Meteor.,* **58,** 19–31.

Dickinson, R. E., A. Henderson-Sellers, P. J. Kennedy, and M. F. Wilson, 1986: Biosphere–atmosphere transfer scheme (BATS) for the NCAR community model. NCAR Tech. Note NCAR/TN-275+STR, 69 pp.

Douville, H., P. Viterbo, J.-F. Mahfouf, and A. C. M. Beljaars, 2000: Evaluation of the optimum interpolation and nudging techniques for soil moisture analysis using FIFE data. *Mon. Wea. Rev.*, **128,** 1733–1756.

Ek, M., and L. Mahrt, 1994: Daytime evolution of relative humidity at the boundary layer top. *Mon. Wea. Rev.*, **122,** 2709–2721.

Eltahir, E. A., 1998: A soil moisture–rainfall feedback mechanism. 1. Theory and observations. *Water Resour. Res.*, **34,** 765–776.

Entekhabi, D., H. Nakamura, and E. G. Njoku, 1994: Solving the inverse problem for soil moisture and temperature profiles by sequential assimilation of multifrequency remotely sensed observations. *IEEE Trans. Geosci. Remote Sens.,* **32,** 438–448.

Fast, J. D., and M. D. McCorcle, 1991: The effect of heterogeneous soil moisture on a summer baroclinic circulation in the central United States. *Mon. Wea. Rev.,* **119,** 2140–2167.

Fennessy, M. J., and J. Shukla, 1999: Impact of initial soil wetness on seasonal atmospheric prediction. *J. Climate,* **12,** 3167–3180.

Fouquart, Y., and B. Bonnel, 1980: Computations of solar heating of the earth's atmosphere: A new parameterization. *Contrib. Atmos. Phys.*, **53,** 35–62.

Frank, W. M., 1983: The cumulus parameterization problem. *Mon. Wea. Rev.*, **111,** 1859–1871.

Fritsch, J. M., and C. F. Chappell, 1980: Numerical prediction of convectively driven mesoscale pressure systems. Part I: Convective parameterization. *J. Atmos. Sci.,* **37,** 1722–1733.

Gallus, W. A., Jr., and M. Segal, 2000: Sensitivity of forecast rainfall in a Texas convective system to soil moisture and convective parameterization. *Wea. Forecasting,* **15,** 509–525.

Garand, L., 1983: Some improvements and complements to the infrared emissivity algorithm including a parameterization of the absorption in the continuum region. *J. Atmos. Sci.*, **40,** 230–244.

Giard, D., and E. Bazile, 2000: Implementation of a new assimilation scheme for soil and surface variables in a global NWP model. *Mon. Wea. Rev.*, **128,** 997–1015.

Grasso, L. D., 2000: A numerical simulation of dryline sensitivity to soil moisture. *Mon. Wea. Rev.*, **128,** 2816–2834.

Habets, F., and Coauthors, 1999: The ISBA surface scheme in a macroscale hydrological model applied to the Hapex–Mobilhy area. Part II: Simulation of streamflows and annual water budget. *J. Hydrol.*, **217,** 97–118.

Hess, R., 2001: Assimilation of screen-level observations by variational soil moisture analysis. *Meteor. Atmos. Phys.,* **77,** 145–154.

Hu, Y., X. Gao, W. J. Shuttleworth, H. Gupta, J.-F. Mahfouf, and P. Viterbo, 1999: Soil-moisture nudging experiments with a single-column version of the ECMWF model. *Quart. J. Roy. Meteor. Soc.,* **125,** 1879–1902.

Huang, J. H., H. M. van den Dool, and K. P. Georgakakos, 1996: Analysis of model-calculated soil moisture over the United States (1931–1993) and applications to long-range temperature forecasts. *J. Climate,* **9,** 1350–1362.

Jacquemin, B., and J. Noilhan, 1990: Sensitivity study and validation of a land surface parameterization using the HAPEX–MOBILHY data set. *Bound.-Layer Meteor.,* **52,** 93–134.

Kasahara, A., 1974: Various vertical coordinate systems used for numerical weather prediction. *Mon. Wea. Rev.,* **102,** 509–522.

Koch, S. E., A. Aksakal, and J. T. McQueen, 1997: The influence of mesoscale humidity and evapotranspiration fields on a model forecast of a cold-frontal squall line. *Mon. Wea. Rev.*, **125,** 384–409.

Lanicci, J. M., T. N. Carlson, and T. T. Warner, 1987: Sensitivity of the Great Plains severe-storm environment to soil-moisture distribution. *Mon. Wea., Rev.*, **115,** 2660–2673.

Laroche, S., P. Gauthier, J. St.-James, and J. Morneau, 1999: Implementation of a 3D variational data assimilation system at the Canadian Meteorological Center. Part II: The regional analysis. *Atmos.–Ocean,* **37,** 281–307.

Mahfouf, J.-F., 1990: A numerical simulation of the surface water budget during HAPEX–MOBILHY. *Bound.-Layer Meteor.,* **53,** 201–222.

——, 1991: Analysis of soil moisture from near-surface parameters: A feasibility study. *J. Appl. Meteor.,* **30,** 1534–1547.

——, and J. Noilhan, 1996: Inclusion of gravitational drainage in a land surface scheme based on the force–restore method. *J. Appl. Meteor.,* **35,** 987–992.

Mailhot, J., R. Sarrazin, B. Bilodeau, N. Brunet, and G. Pellerin, 1997: Development of the 35-km version of the regional finite-element model. *Atmos.–Ocean,* **35,** 1–28.

——, and Coauthors, 1998: Scientific description of RPN physics library. Version 3.6, Recherche en Prévision Numérique, 188 pp. [Available from RPN, 2121 Trans-Canada, Dorval, QC, H9P 1J3, Canada; also available online at http://www.cmc.ec.gc.ca/rpn/physic98.pdf.]

McCorcle, M. D., 1988: Simulation of surface-moisture effects on the Great Plains low-level jet. *Mon. Wea. Rev.,* **116,** 1705–1720.

Mitchell, K., and Coauthors, 2000: The collaborative GCIP land data assimilation (LDAS) project and supportive NCEP uncoupled land-surface modeling initiatives. Preprints, *15th Conf. on Hydrology,* Long Beach, CA, Amer. Meteor. Soc., 1–4.

Molinari, J., and M. Dudek, 1992: Parameterization of convective precipitation in mesoscale numerical models: A critical review. *Mon. Wea. Rev.,* **120,** 326–344.

Noilhan, J., and S. Planton, 1989: A simple parameterization of land surface processes for meteorological models. *Mon. Wea. Rev.,* **117,** 536–549.

——, and P. Lacarrère, 1995: GCM grid-scale evaporation from mesoscale modeling. *J. Climate,* **8,** 206–223.

Paegle, J., K. C. Mo, and J. Nogués-Paegle, 1996: Dependence of simulated precipitation on surface evaporation during the 1993 United States summer floods. *Mon. Wea. Rev.,* **124,** 345–361.

Pal, J. S., and E. A. B. Eltahir, 2001: Pathways relating soil moisture conditions to future summer rainfall within a model of the land–atmosphere system. *J. Climate,* **14,** 1227–1242.

Pan, H.-L., and L. Mahrt, 1987: Interaction between soil hydrology and boundary-layer development. *Bound.-Layer Meteor.,* **38,** 185–202.

Phillips, N. A., 1957: A coordinate system having some special advantages for numerical forecasting. *J. Meteor.,* **14,** 184–185.

Pudykiewicz, J., R. Benoit, and J. Mailhot, 1992: Inclusion and verification of a predictive cloud water scheme in a regional weather prediction model. *Mon. Wea. Rev.,* **120,** 612–626.

Rowntree, P. R., and J. A. Bolton, 1983: Simulation of the atmospheric response to soil moisture anomalies over Europe. *Quart. J. Roy. Meteor. Soc.,* **109,** 501–526.

Schär, C., D. Lüthi, U. Beyerle, and E. Heise, 1999: The soil–precipitation feedback: A process study with a regional climate model. *J. Climate,* **12,** 722–741.

Sellers, P. J., Y. Mintz, C. Sud, and A. Dalcher, 1986: A Simple Biosphere model (SiB) for use within general circulation models. *J. Atmos. Sci.,* **43,** 505–531.

Shukla, J., and Y. Mintz, 1982: Influence of land-surface evapotranspiration on the earth's climate. *Science,* **215,** 1498–1501.

Sud, Y. C., J. Shukla, and Y. Mintz, 1988: Influence of land surface roughness on atmospheric circulation and precipitation: A sensitivity study with a general circulation model. *J. Appl. Meteor.,* **27,** 1036–1054.

Sundqvist, H., 1978: A parameterization scheme for non-convective condensation including prediction of cloud water content. *Quart. J. Roy. Meteor. Soc.,* **104,** 677–690.

Verseghy, D. L., 1991: CLASS—A Canadian land surface scheme for GCMs. I. Soil model. *Int. J. Climatol.,* **11,** 111–133.

Viterbo, P., and A. C. M. Beljaars, 1995: An improved land surface parameterization scheme in the ECMWF model and its validation. *J. Climate,* **8,** 2716–2748.

Wood, E., D. Lettenmaier, and V. Zartarian, 1992: A land surface hydrology parameterization with sub-grid variability for general circulation models. *J. Geophys. Res.,* **97,** 2717–2728.

Yang, R., M. J. Fennessy, and J. Shukla, 1994: The influence of initial soil wetness on medium-range surface weather forecasts. *Mon. Wea. Rev.,* **122,** 471–485.

Zhao, R. J., 1992: The Xinanjiang model applied in China. *J. Hydrol.,* **134,** 317–381.

Ziegler, C. L., W. J. Martin, R. A. Pielke, and R. L. Walko, 1995: A modeling study of the dryline. *J. Atmos. Sci.,* **52,** 263–285.